JOURNAL OF COMPUTATIONAL PHYSICS 119, 271–282 (1995)

Domain Decomposition for Compressible Navier–Stokes Equations with Different Discretizations and Formulations

MOULAY D. TIDRIRI*

ICASE, NASA Langley Research Center, Hampton, Virginia 23681

Received June 2, 1993; revised December 22, 1994

The purpose of this work is to couple different numerical models and approximations for the calculation of high speed external flows governed by the compressible Navier–Stokes equations. The proposed coupling is achieved by the boundary conditions, which impose viscous fluxes and friction forces on the body for the calculation of the global external flow and which impose Dirichlet type boundary conditions on the interface for the local model. © 1995 Academic Press, Inc.

1. INTRODUCTION

The purpose of this work is to couple different numerical models for the calculation of high speed external flows. More precisely, we want to be able to introduce a specific treatment of the flow next to the body, this

(i) for numerical purposes, in order to use locally a different solver (centered scheme, for example);

(ii) for approximation purposes, in order to use locally a much finer grid;

(iii) for physical reasons, in order to use locally a different equation such as nonequilibrium chemical models or Boltzmann kinetic models.

We treat in this paper only the first two aspects. For the third one, we refer to Le Tallec and Tidriri (see [5, 6]) and Tidriri [9].

The proposed coupling is achieved by the boundary conditions, which will impose viscous fluxes and friction forces on the body for the calculation of the global external flow and which will impose Dirichlet type boundary conditions at the external boundary of the local model.

A review of the heterogeneous domain decomposition method for convection–diffusion problems was done in [14]. In [14] the authors discuss the coupling of the convection–diffusion equation with the convection one through proper interface conditions and without overlapping. The purpose here, in our work, is to introduce a specific treatment of the flow next to the body using overlapping techniques. And the resulting algorithm is more general (see [3–6, 9–10]).

* Current address: Yale University, New Haven, CT 06520. This work was done in 1991, at MENUSIN (INRIA, Paris), while the author was a graduate student and was supported by the Hermes Research program under Grant number RDAN 86.1/3. The author was supported by the National Science Foundation under Contract number ECS-8957475 and by the United Technologies Research Center. Present email: tidriri@icase.edu. The author is presently supported by the National Aeronautics and Space Administration under Contract number NAS1-19480.

2. DESCRIPTION OF THE COUPLING STRATEGY

2.1. Navier–Stokes Equations

Let us consider the compressible Navier–Stokes equations which we formally write either as

$$\frac{\partial W}{\partial t} + \operatorname{div}[F(W)] = 0 \quad \text{on } \Omega \text{ (conservative form)}$$

or as

$$\frac{\partial U}{\partial t} + T(U) + D(U) = 0 \quad \text{on } \Omega \text{ (nonconservative form)}$$

with $W = (\rho, \rho v, \rho E)$ and $U = (\rho, v, \theta)$ the conservative and nonconservative variables, $F = F_C + F_D$ the total flux (convective and viscous part), T and D the convective and viscous terms in the nonconservative writing of the Navier–Stokes equations. The problem consists in computing a steady solution of these equations, with boundary conditions

$$\rho v, \rho E \text{ given on } \Gamma_\infty \quad \text{(exterior limit of the domain)},$$

$$\rho \text{ given on } \Gamma_\infty \cap \{x, v(x)\cdot n \le 0\} \quad \text{(inflow)},$$

$$v = 0 \quad \text{on the body } \Gamma_o \text{ (no slip)},$$

$$\theta = \theta_o \quad \text{on the body } \Gamma_o.$$

The global numerical treatment of these equations faces the following difficulties:

—in a conservative calculation, the numerical viscosity of the discretization scheme interferes with the physical viscosity

0021-9991/95 $12.00

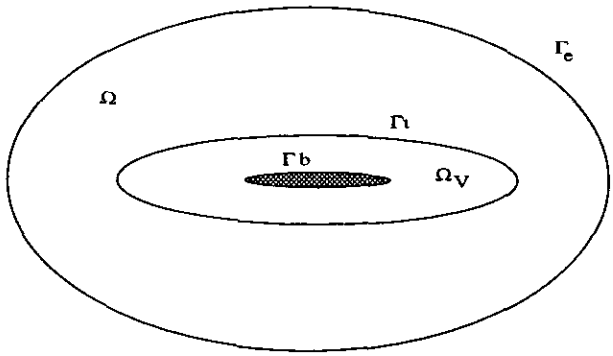

FIG. 1. The global geometry.

and for a mesh of reasonable size leads to an overprediction of the boundary layer. Moreover, no slip boundary conditions on the body are difficult to handle for many TVD schemes;

—in a nonconservative calculation, the correct calculation of a shock requires locally a very fine grid if we want to satisfy the Rankine Hugoniot conditions.

In this framework, our strategy will couple a *global conservative scheme,* defined on the whole domain and based on a finite volume space discretization [1], and a *local approximation,* defined in the neighborhood of the body, which is presently based on a mixed finite element approximation of the nonconservative Navier–Stokes equations [2].

2.2. The General Coupling Strategy

For coupling external Navier–Stokes equations, with local Navier–Stokes equations, we introduce two domains, a global one Ω, a local one Ω_V included in Ω, and an interface Γ_i (Fig. 1 in which Γ_e denotes Γ_∞). The global solution W on Ω and the local solution U_{loc} on Ω_V, which both satisfy the Navier–Stokes equations, are matched by the following boundary conditions, inspired of Schwarz overlapping techniques:

W = given imposed value on Γ_∞,

$n \cdot \sigma(W) \cdot \tau = n \cdot \sigma(U_{\text{loc}}) \cdot \tau$ on the body Γ_o (equality of friction forces)

$q(W) \cdot n + n \cdot \sigma(W) \cdot v = q(U_{\text{loc}}) \cdot n$ on Γ_o (equality of total heat fluxes)

$v \cdot n = 0$ on Γ_o,

$U_{\text{loc}} = 0$ on Γ_o; $U_{\text{loc}} = W$ on the interface Γ_i.

Above, $n \cdot \sigma \cdot n$ and $n \cdot \sigma \cdot \tau$ respectively denote the normal and the tangential force exerted by the body on the flow, with n as the unit normal vector to the body oriented towards its interior.

The calculation of U_{loc} and W satisfying the above boundary conditions is then obtained by the time marching algorithm, which was introduced by Le Tallec and Tidriri (see [3, 4]), and Tidriri [9–11] and which leads to the following algorithm.

Initialization

1. Guess an initial distribution of the conservative variable W in the global domain Ω;

2. Advance in time this distribution by using the global Navier–Stokes solver on N_1 time steps, with *Dirichlet* type boundary conditions on the body Γ_o;

3. Deduce from this result an initial distribution of the local variable U_{loc} on the interface Γ_i and in the local domain Ω_V;

4. Advance in time this distribution by using the local solver on N_2 time steps with Dirichlet boundary conditions on Γ_i and Γ_o.

Iterations

5. From U_{loc}, compute the friction forces $n \cdot \sigma(U_{\text{loc}}) \cdot \tau$ and heat flux $q(U_{\text{loc}}) \cdot n$ on the body Γ_o;

6. Advance the global solution in time (N_1 steps) by using the global Navier–Stokes solver with the above viscous forces as boundary conditions on Γ_o (Section 2.4);

7. From W, compute the value of U_{loc} on the interface Γ_i;

8. Using this new value as Dirichlet boundary conditions on Γ_i, advance the local solution in time (N_2 steps) and go back to step 5 until convergence is reached.

This algorithm completely uncouples the local and the global problems which can therefore be solved by independent solvers. A parallel version is also quite possible, although it is generally wiser to use parallel solvers within steps 6 and 8.

2.3. The Global Navier–Stokes Solver

The global domain Ω is discretized using node centered cells defined on an unstructured grid. Then, at each time step n and for each cell i, we solve

$$\int_{C_i} \frac{W^{n+1} - W^n}{\Delta t} + \sum_{j \in V(i)} \int_{\partial C_i \cap \partial C_j} F_C(W^{n+1}) \cdot n_i + \int_{\partial C_i - \Gamma} F_D(W^{n+1}) \cdot n_i + \int_{\partial C_i \cap \Gamma_\infty} F(W^{n+1}) \cdot n_i = - \int_{\partial C_i \cap \Gamma_o} F_o \cdot n_i.$$

In our numerical implementation, the fluxes F_C and F_D are

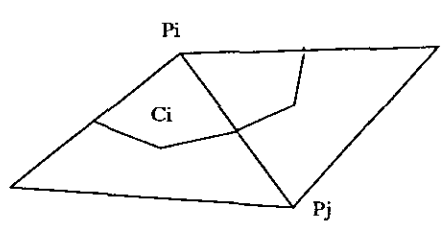

FIG. 2. A boundary cell.

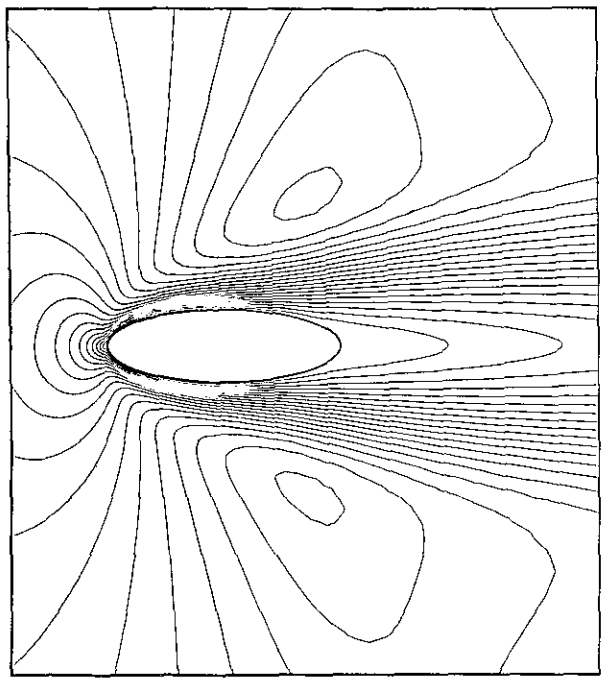

FIG. 3. Mach contours (conservative global computation on domain 2).

computed at time step $n + 1$ and linearized, with F_C computed by an Osher approximate Riemann solver [1]. The resulting linear system is solved by a block relaxation method.

On the body Γ_o, because of our special choice of boundary conditions, the flux is given by

$$\int_{\partial C_i \cap \Gamma_o} F_o \cdot n_i = \int_{\partial C_i \cap \Gamma_o} \begin{pmatrix} 0 \\ n_i \cdot \sigma(W^{n+1}) \cdot n_i \\ n_i \cdot \sigma(U_{\text{loc}}) \cdot \tau_i \\ q(U_{\text{loc}}) \cdot n_i \end{pmatrix},$$

where the aspect of a boundary cell C_i is described in Fig. 2.

In other words, friction forces and heat flux are given explicitly as predicted by the local solver and the mass flux is imposed to zero. Then, in order to have a well-posed problem, at least in the incompressible case (see Section 6), the normal stress (the multiplier of the zero mass flux constraint) cannot be imposed and must be obtained from the solution W^{n+1}.

Remark. Imposing friction forces to the global solution instead of no slip boundary conditions allows to have an accurate solution away from the boundary layer even with a coarse mesh (see [9]).

2.4. Interpretation

The final question concerns the interpretation of the coupled problem solved at convergence in Section 2.2. In a Navier–Stokes/Navier–Stokes coupling, this interpretation is easy. For very fine discretizations, U_{loc} and W satisfy the same Navier–Stokes equations on Ω_V and, at convergence, they satisfy the boundary conditions

$$W = U_{\text{loc}} \text{ on } \Gamma_i,$$
$$q(W) \cdot n + n \cdot \sigma(W) \cdot v = q(U_{\text{loc}}) \cdot n + n \cdot \sigma(U_{\text{loc}}) \cdot v_{\text{loc}} \text{ on } \Gamma_o,$$
$$n \cdot \sigma(W) \cdot \tau = n \cdot \sigma(U_{\text{loc}}) \cdot \tau \text{ on } \Gamma_o,$$
$$v \cdot n = v_{\text{loc}} \cdot n = 0 \text{ on } \Gamma_o.$$

From this, we deduce that W and U_{loc} are solutions of the same well-posed problem defined on Ω_V by the Navier–Stokes equations and by the above boundary conditions. Hence we have $W = U_{\text{loc}}$ on Ω_V which implies that W satisfies the no slip boundary conditions $W = U_{\text{loc}} = 0$ on Γ_o (more precisely, $W = (\rho, \rho v, \rho E) = (\rho, 0, \rho c_v \theta_o)$ on Γ_o). Since W also satisfies by construction the inflow boundary conditions on Γ_∞ and the Navier–Stokes equations on Ω, we finally see that W is the solution of our original problem.

If the discretization step is not very fine, then W and U_{loc} are only identical within the discretization error, an error which is produced first by the coarse mesh used for computing W and second by the weak treatment of the boundary conditions imposed at the wall to W. Because of this weak treatment, the discretization error on W is hoped to stay local, which means that we hope that W will be reliable on the interface. If this is the case, U_{loc} will satisfy the right equation inside Ω_V and the

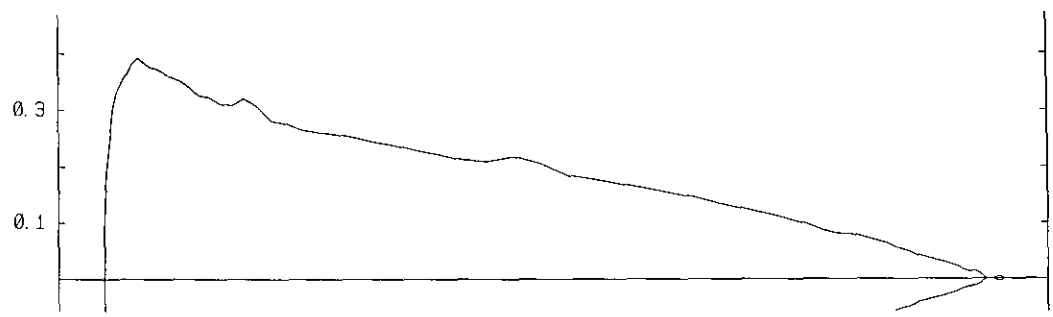

FIG. 4. Skin friction coefficient Cf on the body (conservative global computation on domain 2).

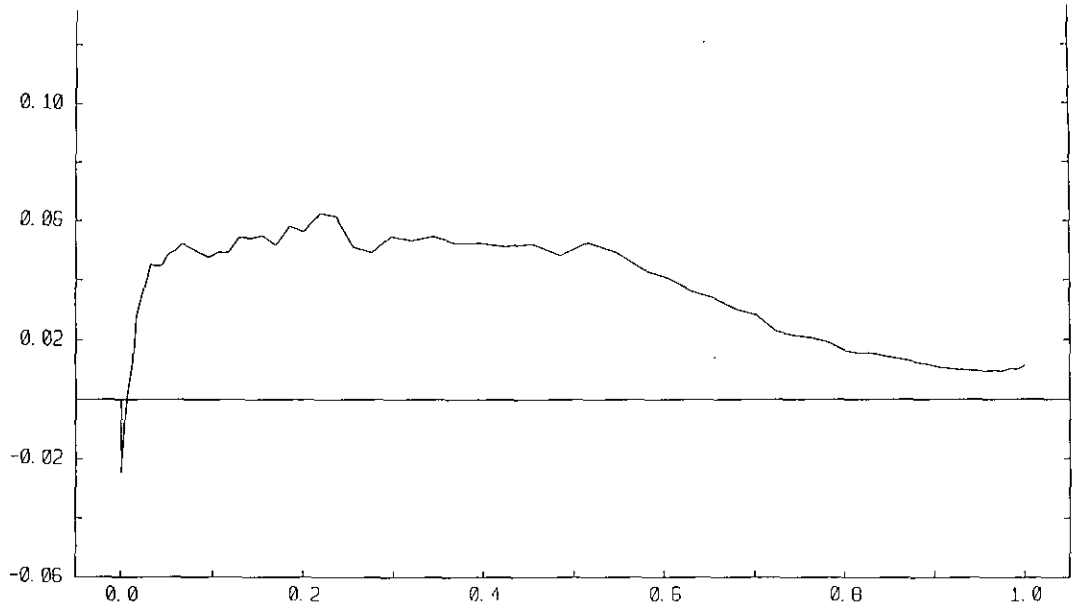

FIG. 5. Stanton number (conservative global computation on domain 2).

right boundary conditions on the interface and on the wall; it should then be an accurate local approximation of the solution.

3. COUPLING CONSERVATIVE AND NONCONSERVATIVE SCHEMES

3.1. The Local Solver

In this case, the local solver takes the form

- let $U^\circ = (\rho, v, \theta)$ be computed at the previous call of the local solver;
- let $U_i = (\rho, v, \theta)$ on Γ_i be computed by interpolation from the values of the global solution W on the interface;
- for $n = 0$ to N_2, solve the local nonconservative Navier–Stokes equations

$$\int_{\Omega_v} \frac{U^{n+1} - U^n}{\Delta t} \cdot \hat{U}_j + \int_{\Omega_v} (T + D)(U^{n+1}) \cdot \nabla \hat{U}_j = 0, \quad \forall j$$

$$U^{n+1} = U_i \quad \text{on } \Gamma_i,$$

$$(v^{n+1}, \theta^{n+1}) = (0, \theta_o) \quad \text{on } \Gamma_o.$$

Here the nonconservative Navier–Stokes equations are discretized by mixed finite elements (P_1 for ρ and θ, P_1 on the subdivided P_2 grid for the velocity). The test functions $\hat{U}_j$ correspond then to the shape functions of the corresponding finite element spaces. The resulting nonlinear system is solved by a few steps of a nonlinear matrix-free Newton/Krylov solver, in which the

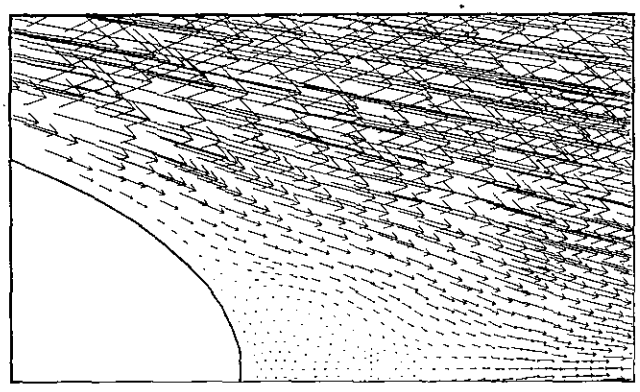

FIG. 6. Velocity field in the wake (conservative global computation on domain 2).

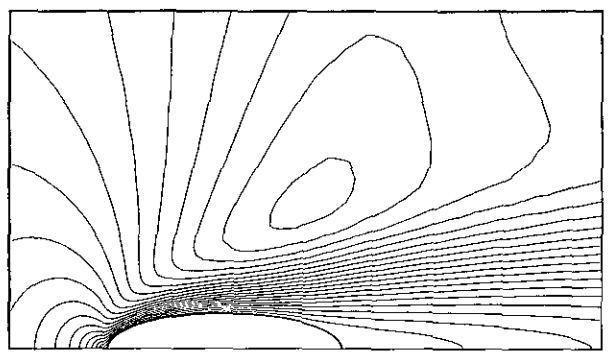

FIG. 7. Mach contours (nonconservative global computation on domain 2).

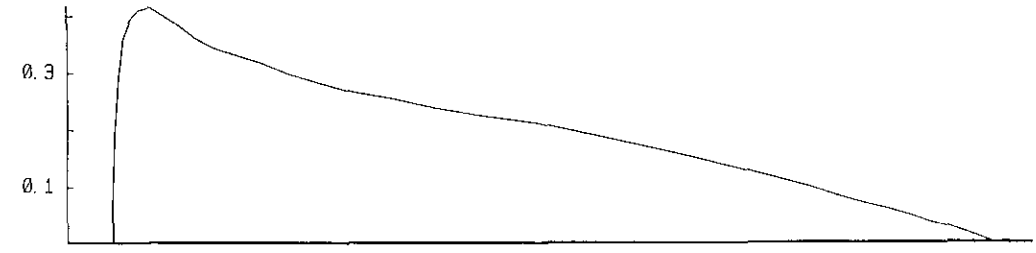

FIG. 8. Skin friction coefficient Cf on the body (nonconservative global computation on domain 2).

Krylov method is GMRES (see [8]). This matrix-free method (which allows no-storage of the matrix) was first proposed and used to solve ODE (see [7]). A more standard way of preconditioning a nonlinear system is to use the usual incomplete factorization techniques such as the incomplete LU (ILU). However, this approach requires the Jacobian matrix explicitly and thus loses the main advantage of Jacobian-free Krylov subspace methods. Therefore we propose to use only diagonal preconditioner. (See [9] for more details.)

In the output, friction forces and heat flux are given by

$$\sigma(U_{\text{loc}}) = \mu(\theta^{n+1})((\nabla v^{n+1} + \nabla^t v^{n+1})/2 - \tfrac{1}{3}\text{div}\, v^{n+1} Id),$$

$$q(U_{\text{loc}}) = \lambda \frac{\partial \theta^{n+1}}{\partial n}.$$

Remarks. (i) The Dirichlet condition on the interface Γ_i can be replaced by a Neumann-type boundary condition of the form

$$(T + D)(U^{n+1}) = g(W) \quad \text{on } \Gamma_i.$$

Such a condition might lead to an easier local problem, since it does not impose a fixed value of the density on an outflow boundary. These ideas have been exploited while coupling different equations such as Navier–Stokes or Euler with the Boltzmann equations (see [9, 12]).

(ii) The nonconservative approach simplifies the calculation of the viscous terms and is well suited to flows at low Mach numbers. On the other hand, it cannot treat hypersonic situations. Therefore, we will also use a conservative local solver (see Section 4).

3.2. Numerical Tests

3.2.1. *The Transonic Case*

The test problem consists of a two-dimensional flow around an ellipse, with 0° angle of attack, $M_\infty = 0.85$, Reynolds number = 100, and a wall temperature $T_W = 2.82T_\infty$.

We have first performed a calculation on a domain which is 8 times larger than the obstacle (we call this domain: domain 1), both with the conservative and the nonconservative schemes. The Mach contours obtained by these calculations are very different (see [9]). We have concluded that this difference is attached to the subsonic character of the flow: Dirichlet boundary conditions imposed on the external boundary of the domain has an influence on the whole flow and this influence is more

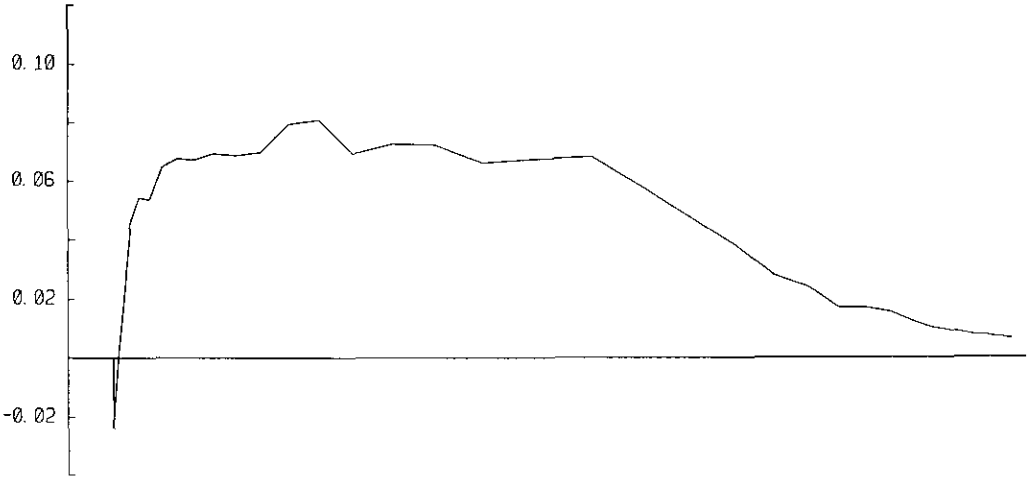

FIG. 9. Stanton number (nonconservative global computation on domain 2).

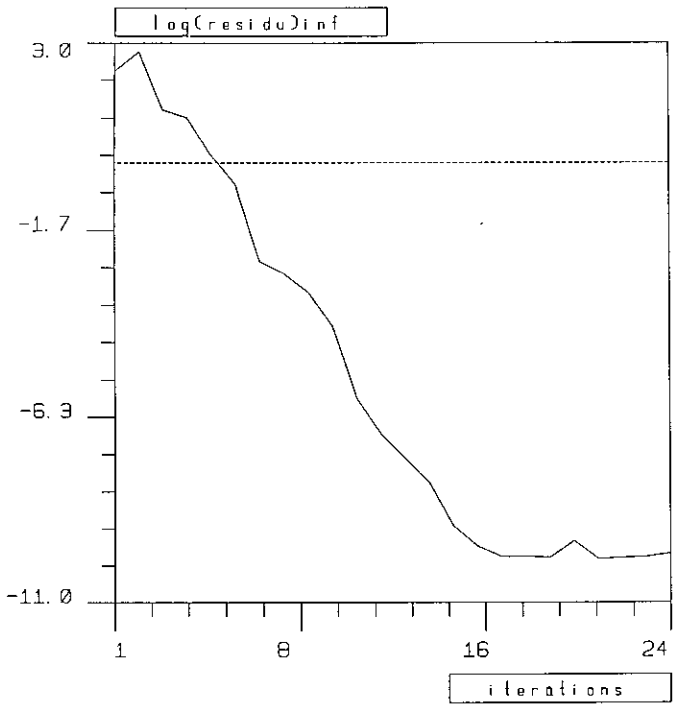

FIG. 10. History of convergence for the coupled approach.

clear in the case of the nonconservative centered scheme. This difference disappears when the computational domain is bigger than 20 times the length of the obstacle (domain 2).

Since all the results presented here, except those of Section 4.2.2, are geometrically symmetrical, we show only on the results above the axis Figs. 3, 13, and 14.

(a) *Conservative global computation on domain* 2. We solve the Navier–Stokes equations with no-slip boundary conditions using the global conservative scheme alone. The mesh has 16,008 nodes and 31,768 elements. Subsequently, this will be our reference. The reference numerical results are shown in Figs. 3 (Mach contours), 4 (skin friction coefficient Cf on the body), 5 (Stanton number Sn), and 6 (velocity field in the wake). We observe small vortices in the wake which can only be detected by a fine mesh and very large viscous effects.

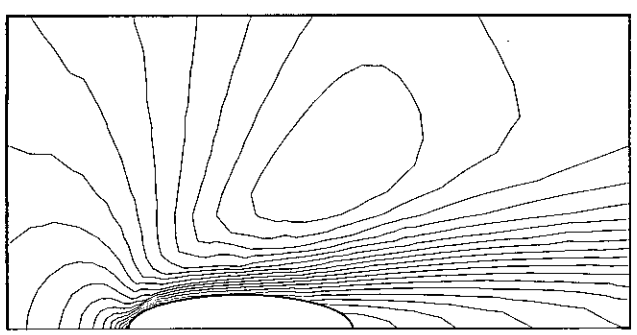

FIG. 11. Mach contours (global computation in the coupled scheme).

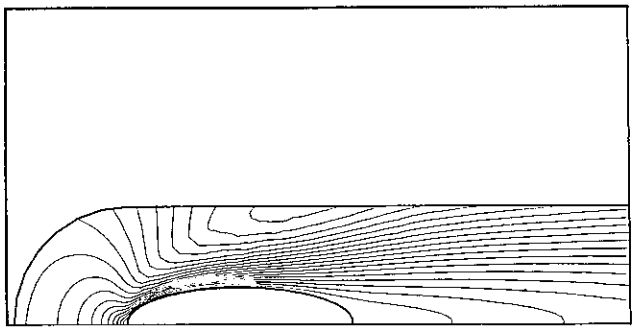

FIG. 12. Mach contours (local computation in the coupled scheme).

(b) *Nonconservative global computation on domain* 2. We solve the Navier–Stokes equations with no-slip boundary conditions by using the global nonconservative solver alone. The mesh used has 4033 nodes and 7942 elements for the P1 grid and 16,184 nodes and 32,120 elements nodes and 7942 elements for the P1 grid and 16,184 nodes and 32,120 elements for the grid P2. The results of this calculation are reported in Figs. 7–9 (Mach contour, Cf, Sn).

As for the global nonconservative calculation (above) and the global conservative calculation they are both perfect for the Mach contours and for the Cf (less than 3% error), but overshoot the maximum value for Sn. This indicates that the temperature grid is too coarse. If we now decrease the size of

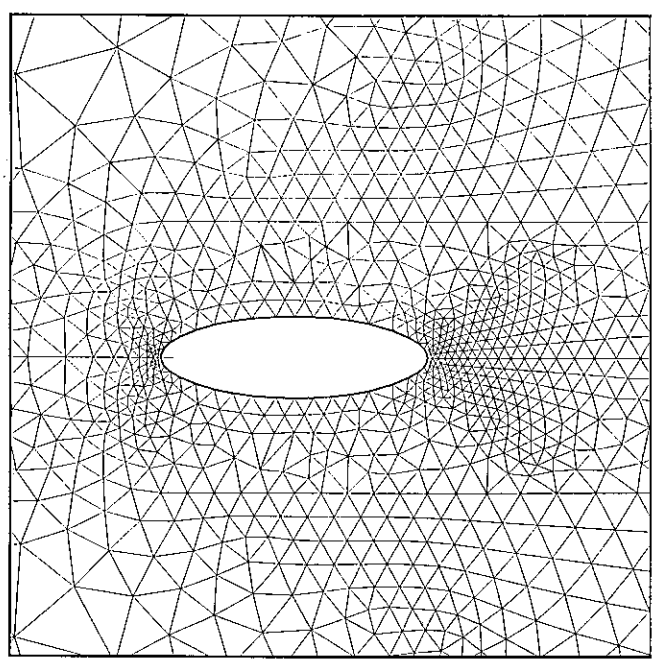

FIG. 13. Zoom of the global mesh.

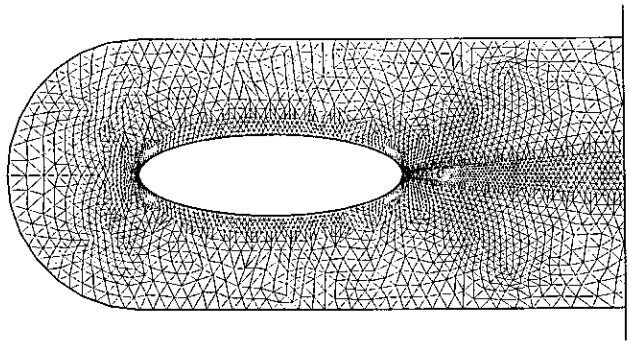

FIG. 14. Zoom of the local mesh.

the computational domain to less than 20 times the length of the obstacle, the global nonconservative calculation is very rapidly polluted, which is not the case for the coupled problem (see below and also [9, 10]).

(c) *Coupled strategy and local refinement techniques.* We solve the Navier–Stokes equations by using the coupled scheme, and taking as the computational domain the domain 1. We take the same global mesh as above (1378 nodes and 2662 elements). For the local domain the mesh has 1114 nodes and 4282 elements. The latter is obtained from an initial local mesh (669 nodes and 1222 elements) by refining adaptively in

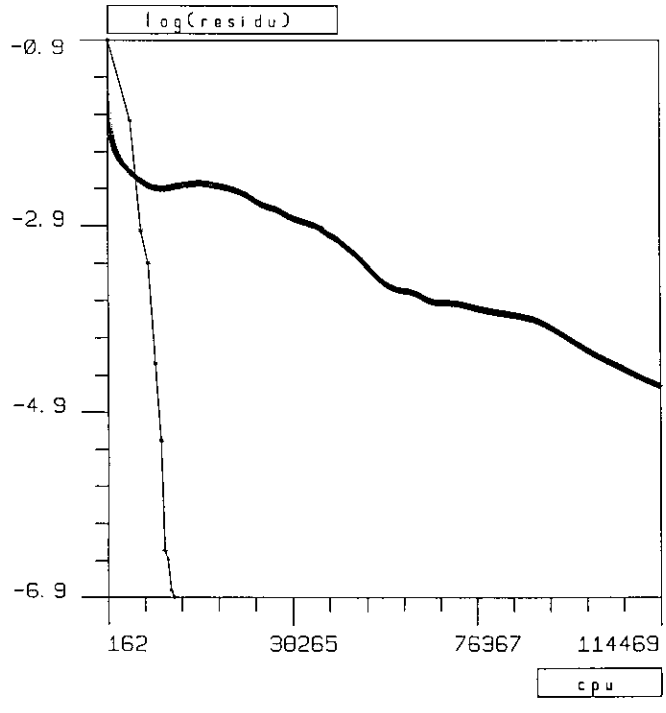

FIG. 15. CPU time comparisons between the uncoupled scheme and the coupled approach. Thin line, coupled scheme; thick line, uncoupled nonconservative scheme.

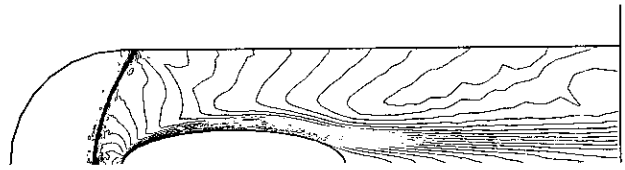

FIG. 16. Mach contours (local computation in the coupled scheme).

the boundary layer and in the wake region. Before refinement, the local results are not sufficiently accurate [9]. Near the body we present the following results:

(1) The Mach contour obtained at convergence in the global calculation (conservative scheme with imposed flux on the body) (Fig. 11).

(2) The Mach contour obtained at convergence in the local computation (nonconservative scheme with imposed boundary conditions on the interface) (Fig. 12).

The Mach contour obtained by the coupled nonconservative scheme (Fig. 12) and by the nonconservative scheme used alone (Fig. 7) are both perfect.

The same conclusion is still valid for both the skin friction and the Stanton number (see [9, 10]).

On Figs. 13 and 14 we show a zoom of the global mesh and of the local one. We remark the incompatibility of the two meshes.

(d) *A Remark on History of Convergence.* We show the history of convergence for the coupled approach, using local time steps:

$$\left\| \frac{\rho^{n+1} - \rho^n}{\Delta t} \right\|_{L^\infty(\Gamma_i)}.$$

This is reported in Fig. 10 for the calculation of (c).

(e) *CPU Time comparison.* On Fig. 15, we show CPU time comparisons. The first curve represents the CPU time function of the residual norm (matrix-free Newton/Krylov) for the nonconservative scheme used alone and corresponds to the calcula-

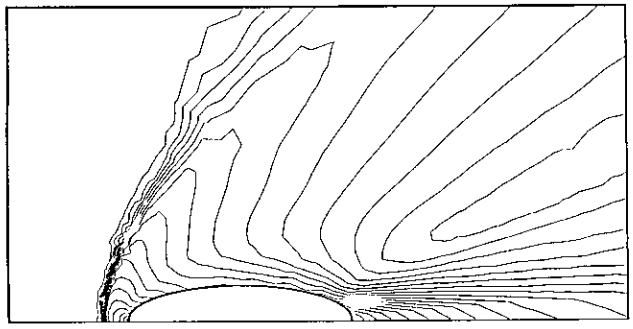

FIG. 17. Mach contours (global computation in the coupled scheme).

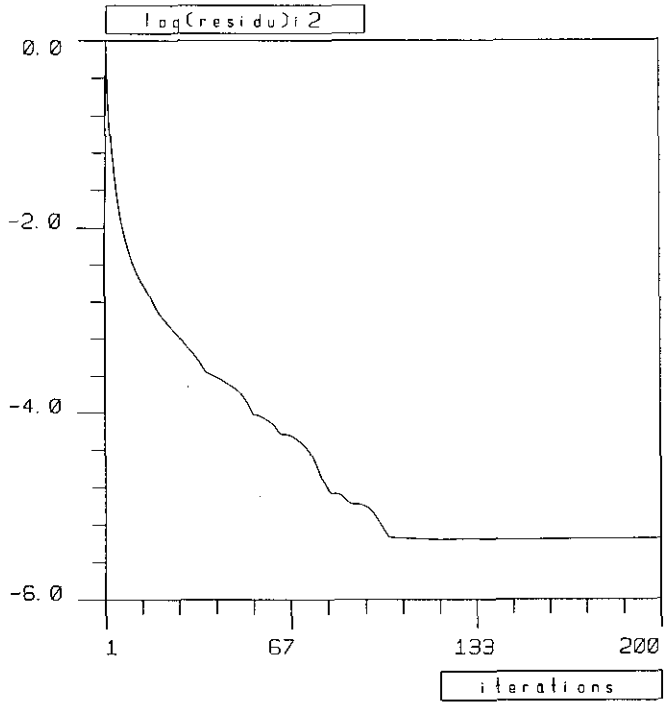

FIG. 18. History of convergence for the coupled approach.

tion of (b). The second curve represents the CPU time function of the residual norm for the coupled approach and corresponds to the calculation of (c). These calculations were done on an Apolo DN 10000. This comparison highlights the high performance of our strategy in terms of CPU time.

3.2.2. *Hypersonic Case*

In this case, the test problem consists of a two-dimensional flow around an ellipse, with 0° angle of attack, $M_\infty = 2$, and $\mathrm{Re} = 1000$. We solve the Navier–Stokes equations with the proposed coupled approach. The local mesh has 3031 nodes and 5834 elements for the grid P1, and 11,896 nodes and 23,336 elements for the grid P2, while the global mesh has only 2510 nodes and 4916 elements.

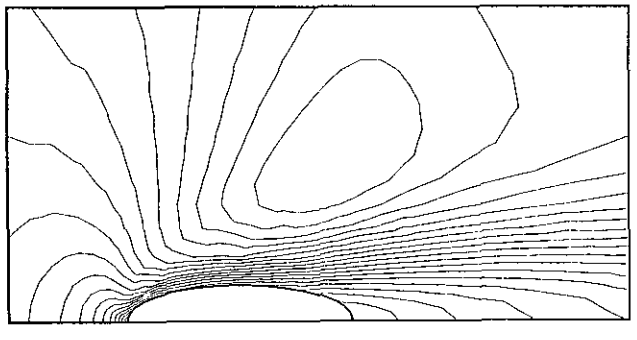

FIG. 19. Mach contours (global computation in the coupled scheme).

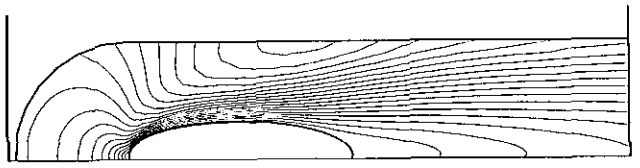

FIG. 20. Mach contours (local computation in the coupled scheme).

Near the body, we present the following results:

(1) The Mach contour obtained at convergence in the nonconservative local calculation with imposed boundary conditions on the interface (Fig. 16);

(2) The Mach contour obtained at convergence in the conservative global calculation with imposed fluxes on the body (Fig. 17).

We remark the importance of the slip phenomenon (see [9]) due to the strong incompatibility of the two meshes (local and global). Finally, we present in Fig. 18 the history of convergence for the coupled scheme:

$$\left\| \frac{\rho^{n+1} - \rho^n}{\Delta t} \right\|_{L^2(\Gamma_i)} \Big/ \left\| \frac{\rho^0}{\Delta t} \right\|_{L^2(\Gamma_i)}.$$

For the same test problem, we have constructed a global mesh such that its trace on the local domain produces the same

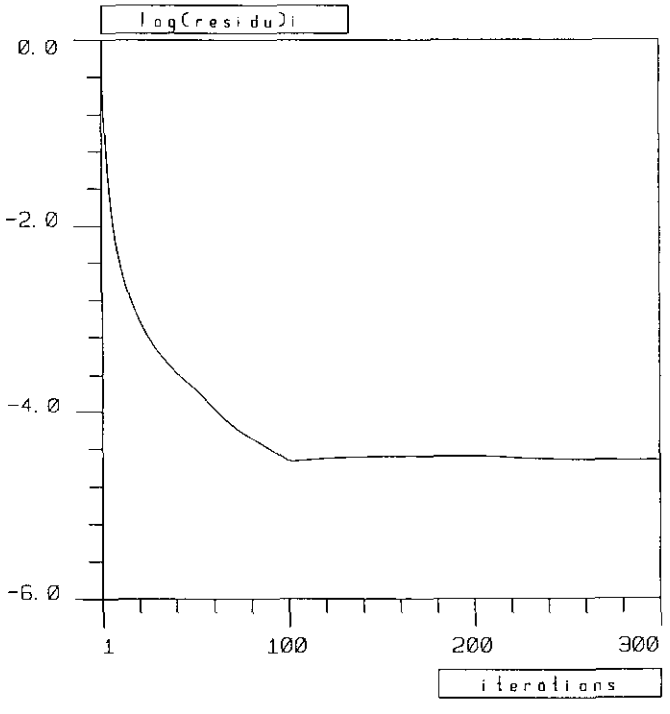

FIG. 21. History of convergence for the coupled scheme.

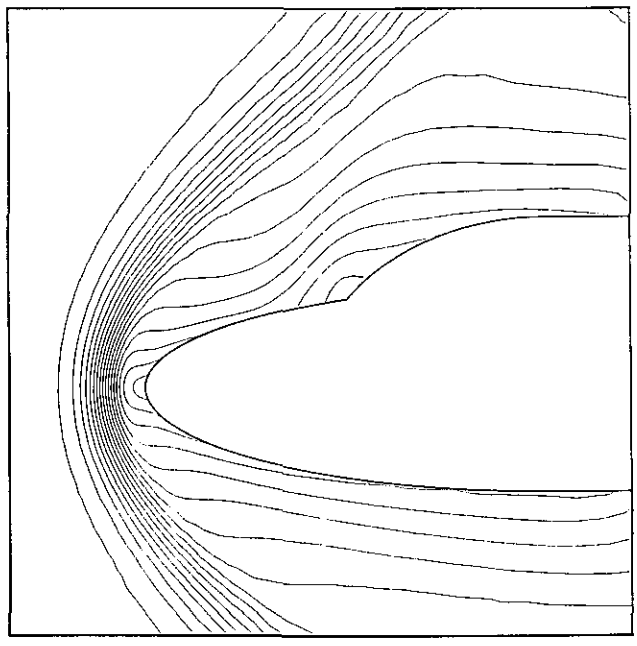

FIG. 22. Mach contours (global computation in the coupled scheme).

local mesh used above, and its trace on the rest of the domain (outside the local part) is four times finer than the corresponding trace of the mesh used for the global calculation in the coupled scheme. This mesh has 4859 nodes and 9578 elements for the grid P1, 19,296 nodes and 38,312 elements for the grid P2. We tried then to use the nonconservative scheme alone for the calculation of the test problem defined above. This scheme did not converge. This shows that our algorithm does make the nonconservative scheme converge, while used alone this same nonconservative scheme does not converge.

Remark 3.1. This test problem shows how the proposed approach extends the validity of the local model.

3.2.3. *Conclusions*

Compared to the global nonconservative approach, the coupled approach is more robust and can use much smaller computational domains.

Compared to the global conservative approach, the coupled method requires fine grids in much smaller regions and allows a large flexibility in the definition of boundary conditions. This flexibility will even be larger for the coupling of differents equations such as Navier–Stokes with Boltzmann (see [5, 6, 9]).

The second conclusion concerns the use of adaptive mesh techniques. The proposed method allows the use of these techniques on the local mesh and hence on a very small domain. Consequently, the proposed method allows the efficient use of these techniques.

The last conclusion concerns the use of the proposed approach in the calculation of hypersonic flows. For the test problem above we have showed that the nonconservative scheme used in our strategy gives good results while the same scheme used alone does not converge. Consequently our method extends the validity of the nonconservative model.

4. COUPLING CONSERVATIVE SCHEMES

In this case the nonconservative local solver is replaced by a conservative one.

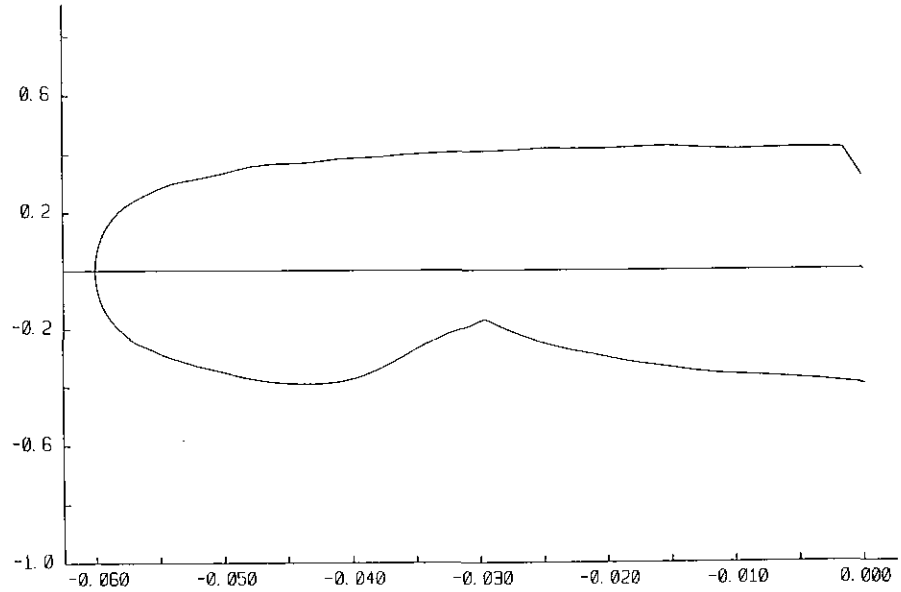

FIG. 23. Tangential velocity on the body (global computation in the coupled scheme).

4.1. The Local Solver

The local solver takes the following form:

• Let $W^0_{\text{loc}} = (\rho, \rho v, e)$ be computed at the previous call of the local solver;

• let $W_i = (\rho, \rho v, e)$ on Γ_i be computed by interpolation from the values of the global solution W on the interface;

• for $n = 0$ to N_2, solve the local conservative Navier–Stokes equations:

$$\begin{aligned}
&\int_{C_i} \left(\frac{W^{n+1}_{\text{loc}} - W^n_{\text{loc}}}{\Delta t} \right)_i dx + \sum_{j \in V(i)} \int_{\partial S_{ij}} F_C(W^{n+1}_{\text{loc}}) \cdot n_i \, d\sigma \\
&\quad + \int_{\partial C_i \cap \Gamma} F_C(W^{n+1}_{\text{loc}}) \cdot n \, d\sigma + \int_{\partial C_i \cap \Gamma} F_D(W^{n+1}_{\text{loc}}) \cdot n \, d\sigma \\
&\quad = 0 \quad \forall i \text{ (cell)} \qquad (1) \\
&W^{n+1} = W_i \quad \text{on } \Gamma_i, \\
&(\rho v^{n+1}, T^{n+1}) = (0, T_b) \quad \text{on } \Gamma_b.
\end{aligned}$$

Here, the conservative Navier–Stokes equations are discretized by the hybrid scheme (finite volume/Galerkin) already used for the global problem.

If we were using compatible meshes for the local and for the global problems, then the coupled approach will yield the results of a global conservative approach. But below, we will use a fine local mesh generated independently on the global mesh.

4.2. Numerical Results

4.2.1. *The Transonic Case*

We treat here the same problem as the one already studied in Section 3. The local mesh used here is obtained from the local mesh used in Section 3. To construct this mesh, we have used an adaptive mesh techniques (see [13]), refining both the boundary layer and the wake region (4282 nodes and 8216 triangles). Near the body we show:

(i) the converged Mach contour in the global conservative solver with imposed fluxes on the body (Fig. 19),

(ii) the converged Mach contour in the local conservative solver with the imposed conditions on the interface (Fig. 20).

The local conservative calculation in the coupled conservative/conservative scheme and the local nonconservative calculation in the coupled conservative/nonconservative scheme produces the same Mach contours (Figs. 19 and 12). But the maximum Cf is 0.36 for the first calculation and 0.41 for the second one. The maximum Stanton number goes from 0.08 for the local nonconservative solver in the coupled conservative/nonconservative to 0.053 for the local conservative solver in the coupled conservative/conservative scheme (see [9, 10]).

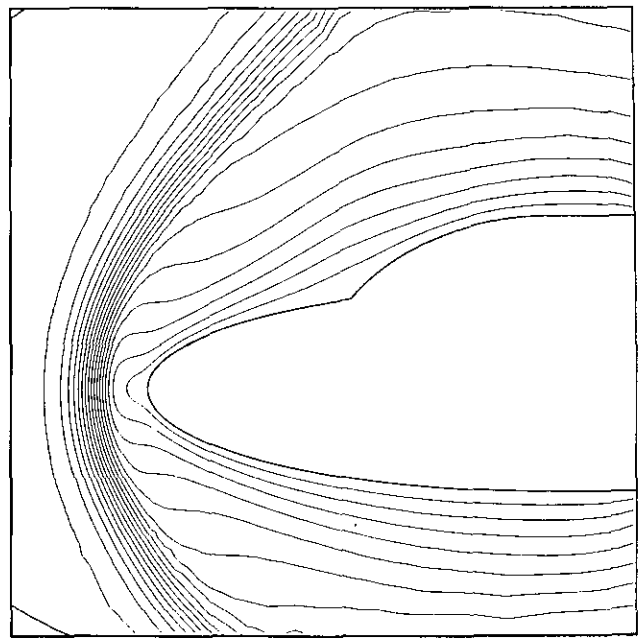

FIG. 24. Mach contours (local computation in the coupled scheme).

A remark on history of convergence. Figure 21 presents the history of convergence; both solvers use local time steps:

$$\|\rho^{n+1} - \rho^n\|_{L^2(\Gamma_i)} / \|\rho^n\|_{L^2(\Gamma_i)}.$$

We show (see [9]) that the coupled scheme does not disturb the history of convergence for the global solver.

A remark on the initialization process. In principle, we initialize the coupled scheme by a uniform flow. Sometimes it is useful to initialize this algorithm by several iterations of the Navier–Stokes calculation with no-slip conditions (see [9] for further details).

4.2.2. *The Hypersonic Case*

The test problem in this case is a calculation around a double ellipsoid with no angle of attack, $M_\infty = 4$ and $\text{Re} = 1000$. The global mesh uses 2749 nodes and 5288 triangles and the local mesh uses 5592 nodes and 10,585 triangles. The latter is obtained by using adaptive mesh techniques refining both the boundary layer and the shock zone.

Near the body, we show:

(i) The converged Mach contour for the global conservative solver with imposed fluxes (Fig. 22).

(ii) The converged Mach contour for the local conservative solver with imposed conditions on the interface Γ_i (Fig. 23).

On Fig. 24 we represent the tangential velocity computed on the body by the global solver. These values are important,

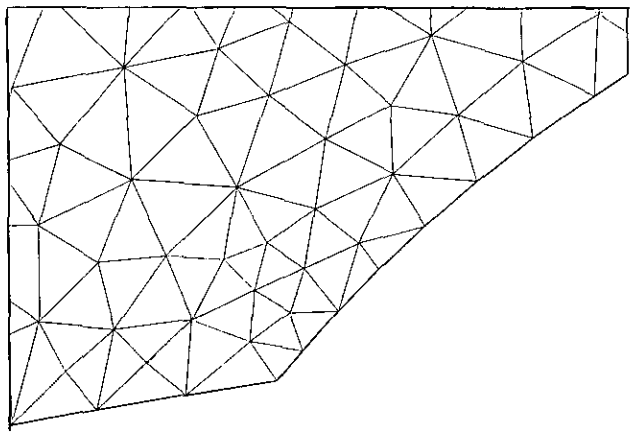

FIG. 25. Loop of the global mesh.

which means that the global mesh and the local mesh are very incompatible (Figs. 25 and 26). But the Cf are still correctly predicted by the coupled approach, which is not true for a global conservative approach with no-slip boundary conditions (the conservative scheme used alone). In other words, the coupled approach gives both an error estimate and a protection against coarse meshes.

4.2.3. *Conclusions*

The coupling scheme allows us to reduce considerably the computational domain and to obtain the same precision locally; on the other hand, it allows an easy identification of the zones where a fine mesh is necessary and gives a large flexibility in the definition of boundary conditions.

The last conclusion concerns the computation of high Mach number flows. We have obtained good results by our coupled strategy using mesh adaptation techniques locally. The local mesh is very fine while the global one is coarse and therefore these meshes are incompatible. The proposed method allows then the use of a fine mesh only locally.

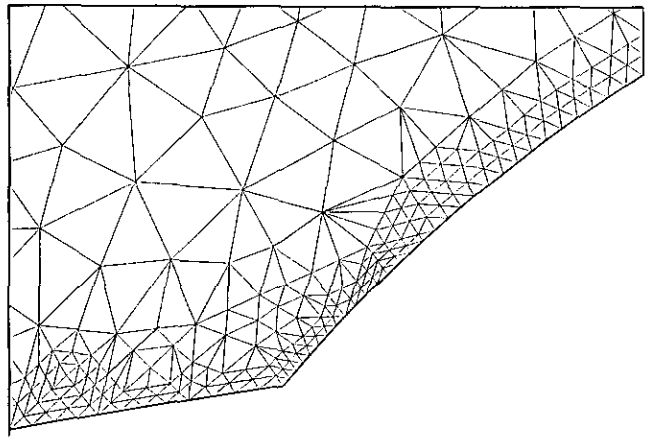

FIG. 26. Loop of the local mesh.

5. CONVERGENCE PROPERTIES OF THE COUPLING SCHEME

As described in [3], numerical tests run for a linear advection diffusion problem show that the coupling algorithm is linearly convergent when Δt is below a limit value which increases with the Reynolds number. A one-dimensional analysis shows that this condition is necessary, an asymptotic analysis done for Δt and h small [9] shows that such a condition is sufficient.

More precisely, if we replace the Navier–Stokes equations by the linear advection diffusion problem

$$\frac{\partial \phi}{\partial t} - \Delta \phi + v \cdot \nabla \phi + \frac{\phi}{\alpha} = 0,$$

$$\phi = \phi_\infty \quad \text{on } \Gamma_\infty,$$

$$\phi = 0 \quad \text{on } \Gamma_o,$$

and if we denote by d the minimal distance from the wall to the interface, we have [4, 9]:

(1) for $\Delta t = \infty$ (that is equivalently if we take N_1 and N_2 to be very large), from the maximum principle, the proposed coupling strategy converges linearly (with constant $K \exp(-d^2/\alpha)$) if d^2/α is large and diverges if $\alpha = 0$ and d small;

(2) for Δt arbitrary, and if we use a time implicit boundary coupling

$$\frac{\partial}{\partial n} W^{n+1} = \frac{\partial}{\partial n} U_{\text{loc}}^{n+1} \quad \text{on } \Gamma_o,$$

the proposed coupling strategy converges linearly. Moreover, a fixed point algorithm applied to the calculation of $(\partial/\partial n) U_{\text{loc}}^{n+1}$ will converge linearly if $d^2/\Delta t$ is sufficiently large;

(3) for Δt arbitrary and time explicit boundary coupling

$$\frac{\partial}{\partial n} W^{n+1} = \frac{\partial}{\partial n} U_{\text{loc}}^{n} \quad \text{on } \Gamma_o,$$

numerical evidence shows that the proposed coupling strategy converges only if Δt is below a certain threshold.

6. THEORETICAL STUDY OF THE BOUNDARY CONDITIONS INTRODUCED BY THE COUPLED STRATEGY: INCOMPRESSIBLE CASE

The theoretical study of the boundary conditions introduced by the coupled strategy shows that each global incompressible Navier–Stokes problem associated with those new slip boundary conditions is well posed. For more details we refer to [9–11].

7. CONCLUSIONS

In this paper we have developed and studied a new algorithm for coupling different discretizations and modelizations. We

have performed extensive study of this algorithm applied to Navier–Stokes equations. We have established the validity of this approach in several configurations (transonic, supersonic, and hypersonic flows).

Compared to classical methods our algorithm allows very much less storage and high performance in terms of CPU time. We have also shown that this algorithm extends the validity of the local model.

The interest of the method to increase accuracy and efficiency by using locally the more appropriate model or approximation has been shown. In addition to these added values in terms of quality and speed, the algorithm gives an easy way of supplementing and testing a large variety of boundary conditions (see [5–6, 9–10, 12]).

ACKNOWLEDGMENTS

I thank my adviser Patrick Le Tallec for the assistance he has given me in revising this paper. This work is based on Chapters 6, 7, and 8, of my Ph.D. thesis [9]. I would like also to think the referees for their comments.

REFERENCES

1. Ph. Rostand and B. Stoufflet, Rapport de recherche INRIA No. 863, July 1988.
2. M. O. Bristeau, R. Glowinski, L. Dutto, J. Périaux, and G. Rogé, "Compressible Viscous Flow Calculations Using Compatible Finite Element Approximations," in *7th Int. Conf. on Finite Element Methods in Flow Problems, Huntsville, Alabama, 1989; Int. J. Numer. Methods Fluids* **11**, 719 (1990).
3. P. Le Tallec and M. D. Tidriri, "Couplage et conditions aux limites, Rapport de contrat," July 1989 (unpublished).
4. P. Le Tallec and M. D. Tidriri, *Math. Comput.*, submitted.
5. P. Le Tallec and M. D. Tidriri, *J. Comput. Phys.*, submitted.
6. P. Le Tallec and M. D. Tidriri, Rapport de contrat HERMES R/Q 6465/91, INRIA, Feb. 1993 (unpublished).
7. P. Brown and Y. Saad, Lawrence Livermore National Laboratory Research Report UNRL-907645, Nov. 1987 (unpublished).
8. Y. Saad and M. H. Schultz, *SIAM J. Sci. Stat. Comput.* **7**, 865 (1986).
9. M. D. Tidriri, thèse, Université de Paris IX, May 1992 (unpublished).
10. M. D. Tidriri, INRIA Research Report RR-2378, October 1994 (unpublished).
11. M. D. Tidriri, *SIAM J. Math. Anal.*, submitted.
12. J. F. Bourgat, P. Le Tallec, F. Mallinger, Y. Qiu, and M. D. Tidriri, Numerical coupling of Boltzmann and Navier–Stokes in *Proceedings of I.U.T.A.M. (International Union of Theoretical and Applied Mechanics) Conference. Marseille, France, Sept. 1–4, 1992.*
13. C. Pouletty, These de Docteur Ingenieur, Ecole Centrale, Dec. 1985 (unpublished).
14. A. Quarteroni, F. Pasquarelli, and A. Valli, *5th International Conference on Domain Decomposition Methods, Norfolk, VA, 1991* (SIAM, Philadelphia, 1991).